

Cite this: *Lab Chip*, 2011, **11**, 921

www.rsc.org/loc

PAPER

Dielectrophoresis–Raman spectroscopy system for analysing suspended nanoparticles†

Adam F. Chrimes,^{*a} Aminuddin A. Kayani,^a Khashayar Khoshmanesh,^b Paul R. Stoddart,^c Paul Mulvaney,^d Arnan Mitchell^a and Kouros Kalantar-zadeh^a

Received 5th October 2010, Accepted 20th December 2010

DOI: 10.1039/c0lc00481b

A microfluidic dielectrophoresis platform consisting of curved microelectrodes was developed and integrated with a Raman spectroscopy system. The electrodes were patterned on a quartz substrate, which has insignificant Raman response, and integrated with a microfluidic channel that was imprinted in poly-dimethylsiloxane (PDMS). We will show that this novel integrated system can be efficiently used for the determination of suspended particle types and the direct mapping of their spatial concentrations. We will also illustrate the system's unique advantages over conventional optical systems. Nanoparticles of tungsten trioxide (WO₃) and polystyrene were used in the investigations, as they are Raman active and can be homogeneously suspended in water.

Introduction

The investigation of suspended micro and nanoparticle properties is of utmost importance for the understanding and determination of their optical, electronic, mechanical and chemical behaviours. These studies are used for answering fundamental questions such as: how particles interact with each other in suspended forms;¹ how they exchange electrons, photons or phonons, when they are in the close affinity to each other in liquid media;^{2,3} and how they interact with the chemical components surrounding them.⁴

The investigation of particles in microfluidics has been carried out using a variety of methods such as resonant light scattering (RLS),⁵ confocal microscopy combined with charged coupled device (CCD) cameras with or without fluorescent particles^{6,7} and PIN-based photo detectors.⁸ However, the capability of these methods for simultaneous *in situ* measurements of both concentration and type of the suspended particles is limited. Even fluorescence microscopy, which is the most investigated method in dealing with such particles, has certain limitations as its capability is restricted to fluorescent materials. As an alternative, Raman spectroscopy allows such assessments and can be

used for the pattern (“fingerprint”) acquisition of Raman active particle suspensions.⁹ Its integration with microfluidics permits the mapping of both the concentration and type of micro and nanoparticles. Additionally, the intensity of Raman peaks is a function of particle concentration and the peak positions identify the material type.

There are recent reports covering a wide range of *in situ* Raman measurement techniques using suspended micro and nanoparticles.^{3,9–15} Of particular interest are works that integrate microfluidics with surface-enhanced Raman scattering (SERS)^{3,10,11,16} and surface-enhanced resonance Raman scattering (SERRS) systems.¹⁷ It has been shown that colloidal silver in microfluidics can be effectively used for *in situ* SERS measurements. This includes the detection of bio-components such as anion activators and pesticides¹⁰ as well as *dipicolinic acid* and *malachite green*.¹⁶ Keir *et al.*¹⁷ used silver colloid generated SERRS for the detection of *trinitrotoluene* (TNT) derivatives. In their report, the particles were focused into the centre of the channel through the use of laminar flow, and Raman spectroscopy was used to determine the concentration of the target analytes. This method achieved a detection limit down to 10 fM. Piorek *et al.*¹ have described a method of using microfluidics and silver SERS nanoparticles, in which *4-aminobenzenethiol* was detected by creating SERS “hot spot” signals. There are also reports on the application of Raman spectroscopy for the determination of the type of colloids in liquids^{16,18} including investigations of *in situ* SERS patterns obtained from gold microparticles.¹⁹ It has been shown that by immobilising different types of biochemical components on gold particles, the Raman peaks change significantly, and are associated with the types of target biomaterials.

All of the abovementioned reports focused on the development of basic microfluidics, and lacked effective methods for the

^aSchool of Electrical and Computer Engineering, RMIT University, Victoria, Australia. E-mail: adam.chrimes@rmit.edu.au; Fax: +61 03 9925 2007; Tel: +61 04 0077 1703

^bCentre for Intelligent Systems Research, Deakin University, Victoria, Australia

^cCentre for Atom Optics and Ultrafast Spectroscopy, Swinburne University, Victoria, Australia

^dSchool of Chemistry and Bio21 Institute, University of Melbourne, Parkville, Victoria, Australia

† Electronic supplementary information (ESI) available: In depth DEP simulations, SEM images of particles, permittivity simulations and concentration discussions. See DOI: 10.1039/c0lc00481b

manipulation of suspended nanoparticles. To circumvent this problem Tong *et al.*²⁰ demonstrated the use of optical tweezers to alter the concentration of colloids and study the effect on SERS signals. However, optical tweezing interferes with the collection of Raman measurements, which could potentially deteriorate the performance of their system. Moreover, optical tweezing requires significant optical intensity, which is unsuitable for constituents at the micron scale or larger. In addition, the application of laminar flow, as suggested by Keir *et al.*,¹⁷ does not provide an effective means for the real time manipulation of suspended nanoparticles. A potential solution is the application of dielectrophoresis (DEP).

Dielectrophoretic manipulations have been widely applied to nano, meso and microscale particles in microfluidics.²¹ By changing the applied voltage and frequency, particles can be focused to, or repelled from pre-determined locations within the microchannel. Such a capability provides a perfect base for the demonstration of microfluidics and Raman spectroscopy as a tool for the mapping, recognizing and measuring of particles. The integration of microfluidics and DEP has been the key in the development of many new and exciting micro-platforms. These platforms have been used in applications such as particle counting,^{6,22} particle sorting of both organic^{23–28} and inorganic^{21,29} particles, opto-fluidics^{30,31} and for the creation of electronic devices.^{32,33} Systems involving DEP and optical measurements incorporate fluorescent particles into the solution, and the fluorescence intensity using a CCD module is measured.⁶ However, to date there are no reports on the integration of DEP and Raman systems for the *in situ* analysis of suspended particles.

In this paper, we show that by integrating Raman spectroscopy with a microfluidic DEP system, the resultant system can be used to map the concentration and type of suspended nanoparticles within the microchannel. To show the functionality of this system, we use DEP to manipulate the nanoparticles, producing regions of high and low particle concentrations within the microchannel. We show that the integration of DEP and Raman spectroscopy can be a powerful tool for the *in situ* analysis of suspended inorganic (WO_3) and organic (polystyrene) particles.

Principles of performance and design

DEP simulations were performed in order to identify the most effective DEP settings for the investigation, and help to explain the particle behaviour inside the microchannel. The dielectrophoretic force experienced by a spherical particle is:^{34,35}

$$F_{\text{DEP}} = 2\pi\epsilon_m r^3 \text{Re}[f_{\text{CM}}(\omega)] \nabla E_{\text{rms}}^2 \quad (1)$$

where ϵ_m is the permittivity of the suspending medium, r is the radius of the particles, $\text{Re}[f_{\text{CM}}]$ is the real part of the Clausius–Mossotti (CM) factor, ω is the angular frequency of the applied signal, and E_{rms} is the root-mean-square value of the induced electric field. The CM factor, which determines the relative polarisability of the particle with respect to the suspending medium, is defined for spherical particles as:³⁵

$$f_{\text{CM}} = \frac{\epsilon_p^* - \epsilon_m^*}{\epsilon_p^* + 2\epsilon_m^*} \quad (2)$$

where ϵ_p^* and ϵ_m^* are the complex permittivities of the particle and suspending medium, respectively, each defined as $\epsilon - i\sigma/\omega$. Depending on the polarity of the f_{CM} , a particle experiences positive or negative dielectrophoretic forces, and consequently is pushed towards or away from the regions of high electric field strength.³⁴ Further simulations and details of the particle behaviour at different DEP frequencies are contained in the ESI†.

In these experiments curved DEP electrodes are used (Fig. 1). This particular design allows control of both hydrodynamic and dielectrophoretic forces to create a highly focused stream of particles in the microchannel.^{21,25,31,36} This is especially important as curved electrodes provide controlled and repeatable areas of high and low particle concentration, without producing turbulent flows near the electrode tips. This is necessary for the successful demonstration of *in situ* Raman spectroscopy. The platform contains 40 electrode pairs spanning the entire length of the microfluidic channel with individual dimensions detailed in Fig. 1(c).

The microfluidic device was a simple rectangular structure, which was formed from poly-dimethylsiloxane (PDMS), and was 1200 μm long, 300 μm wide and 50 μm deep. Two reservoirs were formed at the ends of the channel to introduce and exhaust liquid. The PDMS material forming the walls of the channel exhibit inherent Raman peaks,³⁷ which can interfere with the performance of Raman spectroscopy. To reduce the effect of PDMS interference, the channel floor was formed from a transparent substrate. The electrodes were patterned on this substrate and confocal Raman spectroscopy was performed through the substrate in an inverted configuration (Fig. 1(a) and (b)). This

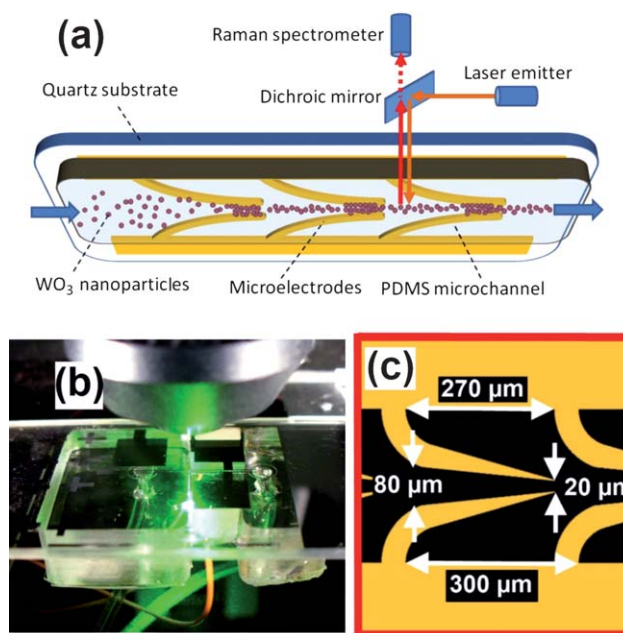


Fig. 1 (a) Schematic of DEP-Raman system layout. (b) Photo of complete DEP-Raman system under test. (c) Curved DEP electrode design and layout.

ensured minimal interfering signal was collected from the PDMS.

Glass is the substrate most favoured for the fabrication of DEP electrodes^{23,24,26,27,38,39} as it is cheap, non-conductive (essential for DEP electrode use), transparent at visible wavelengths and non-reactive to most biological materials. However, glass is Raman active, exhibiting a broad peak at 1000 cm^{-1} .⁴⁰ Other substrates widely used in microfluidics include silicon wafers coated with thin non-conductive silica layers⁴¹ and polymer-based substrates.⁴² However these substrates are also Raman active. Alternatively, quartz was used in this work as the substrate for the electrode patterning. The Raman response of quartz is insignificant compared to the particles of interest.^{43,44} The electrodes were fabricated onto the substrates using photolithography techniques by forming electrodes of 200 nm thickness from the electron beam deposited Au (150 nm)/Cr (50 nm) layers. The PDMS and the substrate were attached together forming a leak proof seal^{33–36,38,39} (see ESI† for the fabrication details).

Numerical analysis of the DEP system

In order to analyse the performance of the system, the dielectrophoretic field was simulated using the Fluent software package (Fluent, Lebanon, NH, USA), as detailed by Khoshmanesh *et al.*³⁶ When a 15 V sinusoidal voltage is applied to the electrodes, the resultant electric field reaches a maximum value of $2.8 \times 10^6\text{ V m}^{-1}$ at the tips, where the gap between the opposite microelectrodes is $20\text{ }\mu\text{m}$ and the width of microelectrodes is reduced to $5\text{ }\mu\text{m}$ (Fig. 2(a)). At low frequencies, the particles exhibit a positive DEP response (Fig. 2 in the ESI†) and are driven towards the microelectrodes, provided that the dielectrophoretic force is strong enough to overcome the sedimentation force, F_{Grav} . The density of particles between the microelectrodes is proportional to the magnitude of $F_{\text{DEP}} - F_{\text{Grav}}$ (Fig. 2(b)). F_{DEP} is proportional to E^2 , as given in eqn (1), and therefore $F_{\text{DEP}} - F_{\text{Grav}}$ increases along the microelectrodes until reaching a peak at the tips. For example, the distribution of $F_{\text{DEP}} - F_{\text{Grav}}$ applied on tungsten trioxide (WO_3) and polystyrene particles at 15 V and 10 MHz is shown at a plane $10\text{ }\mu\text{m}$ from the quartz substrate (Fig. 2b). The WO_3 particles experienced a maximum force of $2 \times 10^{-15}\text{ N}$ at the tips of the electrodes, while the polystyrene particles experienced a maximum force of $2.4 \times 10^{-14}\text{ N}$ due to their larger dimensions (ESI information provided†).

Materials and methods

Initially, silicon nanoparticle suspensions were used inside the microfluidic device. Silicon has an excellent Raman response, with a prominent peak at 520 cm^{-1} and is often used to calibrate Raman systems.⁴⁵ However, silicon nanoparticles were electrostatically attracted to the PDMS channel wall, and gradually led to the build-up of an undesirable background Raman signal.⁴⁶ It was also noted that nanoparticles of zinc oxide (ZnO) and molybdenum trioxide (MoO_3) aggregated at the channel walls, even in the presence of various surfactants. Conversely, WO_3 and polystyrene particles remained colloidally stable within the microfluid system and hence, the results below focus on these two

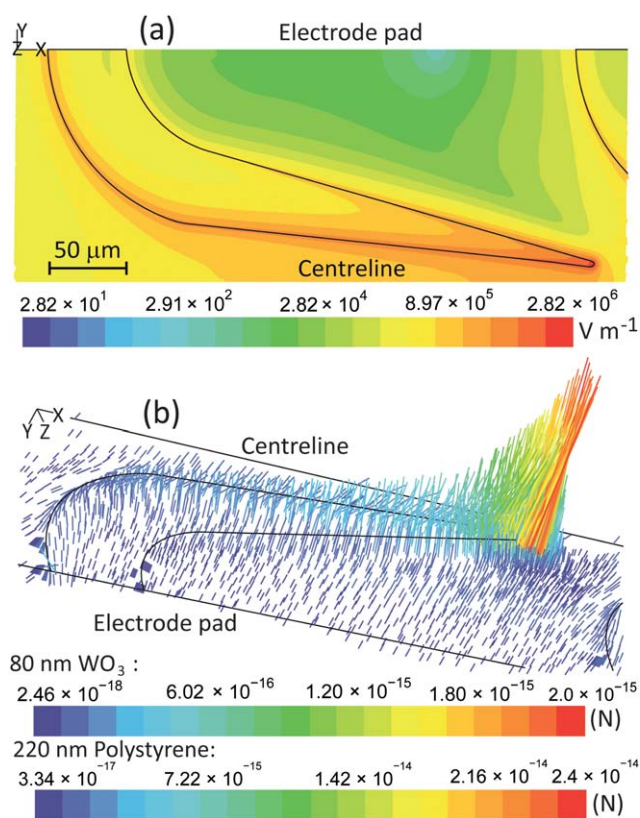


Fig. 2 (a) The contours of electric field (V m^{-1}) at 15 V, and $z = 0\text{ }\mu\text{m}$ (surface of quartz substrate). (b) The vectors of $F_{\text{DEP}} - F_{\text{Grav}}$ (N) applied on WO_3 and polystyrene particles at 15 V and 10 MHz, and $z = 10\text{ }\mu\text{m}$ with respect to the surface of quartz substrate. Vectors are pseudo-coloured and lengthened according to the magnitude of $F_{\text{DEP}} - F_{\text{Grav}}$ force (N).

types of particles. In principle, PDMS can be functionalised with materials such as poly(ethylene glycol) to reduce non-specific nanoparticle binding; however for the proof of principle experiments reported here, this is not necessary.^{47–49}

The DEP-microfluidic chip was trialled with well suspended and controlled WO_3 nanoparticles (diameter $\sim 80\text{ nm}$, 99%, Sigma Aldrich). WO_3 has been studied using Raman spectroscopy in the past and is known to produce several strong peaks.⁵⁰ Additionally, polystyrene nanoparticles (diameter $\sim 220\text{ nm}$, 90%, Bangs Laboratories Inc.) were also investigated, which were pre-suspended in DI water combined with SDS (sodium dodecyl sulfate) surfactant (0.1%) and are surface functionalised with $-\text{COOH}$ groups. Scanning electron microscope (SEM) images of the WO_3 and polystyrene nanoparticles are presented in the ESI†. The particles were suspended in DI water, while Triton X-305 surfactant was also added to improve the homogeneous distribution of particles within the mixture. The mixtures were prepared at concentrations of 6.5% w/w and 1.5% w/w for WO_3 and polystyrene, respectively.

Combined Raman spectroscopy and DEP was used to analyse the mixtures. The investigations were conducted at different electric field frequencies and at different positions within the microchannel. During these experiments, the flow rate was kept constant at $4\text{ }\mu\text{L min}^{-1}$ using a syringe pump (Harvard

Apparatus PHD2000). The magnitude of the applied voltage was also held constant at 15 V throughout each experiment by using a programmable function generator (Tabor Electronics 8200).

An Olympus BX41 confocal microscope, equipped with a Jobin Yvon Horiba TRIAX320 spectrometer and a thermoelectrically cooled CCD detector, was utilised to collect the Raman spectra. The system included a white light source for the back lit upright microscope and a 532 nm laser source (rated power 1.1 mW) as the Raman excitation laser. The microscope objective was a $\times 50$ with a numerical aperture of 0.5. This lens produced an excitation spot approximately $0.65\ \mu\text{m}$ in diameter with a depth of field approximately $8\ \mu\text{m}$. All Raman spectra in this report were captured using a 20 second integration time with an average of 3 integrations, while the pinhole of the microscope was set to $100\ \mu\text{m}$ (unless otherwise stated).

Raman spectra were captured under three different sets of conditions:

(1) The frequency of the applied DEP field was varied, while focusing the Raman microscope focal point onto a constant position within the particle stream.

(2) The vertical location of the Raman microscope lens focal point was changed in depth (by moving the substrate vertically), while applying a fixed dielectrophoretic force.

(3) The Raman spectra were captured at several different locations around the electrodes, while applying a constant voltage and frequency.

Results and discussions

Inverted microscope analysis of DEP platform

Fig. 3 depicts the suspended WO_3 nanoparticles at different applied DEP frequencies. Using DEP, we were able to produce areas of high and low concentrations of particles within the microfluidics. This effect can be clearly seen in the optical images (Fig. 3). The response of the particles relative to the frequency of the applied electric field was predicted using eqn (2) (as shown in the ESI \dagger), assisting us in determining the DEP crossover frequencies for Raman studies. The frequency of the applied field was varied from 20 MHz to 100 kHz in order to observe changes in the Raman spectra of the particles.

At no applied signal, a uniform particle distribution was observed in the microchannel (Fig. 3(a)). At 20 MHz, the WO_3 particles experienced weak DEP forces, and became trapped between the electrode tips. However, the DEP force was not strong enough to hold the particles against the drag force. As a result, most of the trapped particles were washed away, forming a wide stream of particles along the centre-line (Fig. 3(b)). At 10 MHz, the DEP force became stronger and more particles were trapped. It not only extended the effective trapping region of the electrodes but also narrowed the dark particle stream along the centre-line (Fig. 3(c)). At frequencies below 10 MHz (Fig. 3(d)–(f)) the particle stream continued to form along the centre-line. However, as the DEP frequency was reduced further, the particle stream started to disperse as it approached the next electrode pair. This is because at low frequencies the DEP force is intensified, pushing more particles towards the electrodes. However, the particles did not have

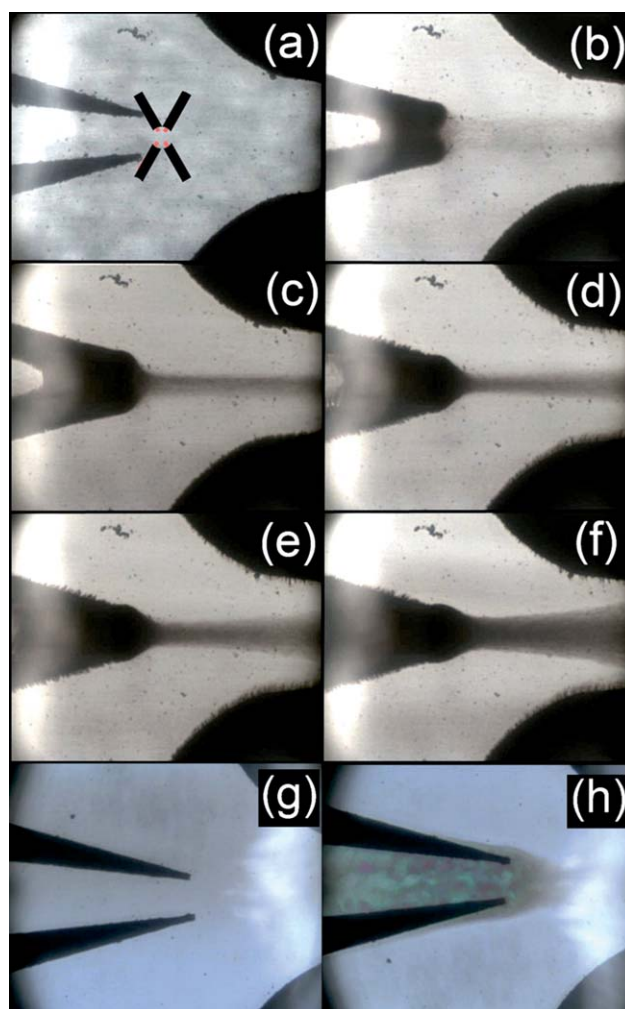


Fig. 3 Inverted microscope images of DEP system with WO_3 nanoparticles at the following frequencies: (a) no-DEP voltage, (b) 20 MHz, (c) 10 MHz, (d) 1 MHz, (e) 750 kHz, (f) 250 kHz; inverted microscope images of DEP system with polystyrene nanoparticles at the following frequencies: (g) no-DEP voltage, (h) 500 kHz.

sufficient time to come to rest between the electrodes due to the high flow rate of the medium.

The behaviour of the WO_3 mixture closely follows the behaviour expected, based on the calculated values of f_{CM} (presented in ESI \dagger). The predicted crossover frequency of 22 MHz is very close to the observed DEP crossover at 20 MHz, which shows a weak stream of particles along the centre-line.

Fig. 3(g) depicts the polystyrene mixture in the no-DEP voltage condition, in which particles were evenly distributed. Alternatively, Fig. 3(h) depicts the polystyrene nanoparticle mixture when exposed to a DEP voltage of 15 V at 500 kHz. A clear narrow band in the middle cannot be observed; however, the region between the electrodes exhibits diffraction due to the local ordering of the polystyrene particles. The refractive index of polystyrene is ~ 1.58 , which is much closer to that of water ~ 1.33 in comparison to WO_3 (~ 2.3).^{51,52} The smaller refractive index difference between the polystyrene nanoparticles and water makes it difficult to see any narrow band formed, hence only the two extreme cases (no DEP and strong trapping DEP force at 500 kHz) are shown.

Raman microscopic analysis at differing DEP settings

The focal point of the Raman microscope lens was placed immediately after the two electrode tips (as shown in Fig. 3(a)) and Raman spectra of suspended WO_3 (Fig. 4) and polystyrene (Fig. 5) were collected. The measurements were conducted when the electrodes were in optical focus, the condition which we refer to as the “top surface of the microchannel” in the rest of this text.

WO_3 exhibits two strong Raman peaks at 707 and 798 cm^{-1} , caused by the $\nu(\text{O}-\text{W}-\text{O})$ stretching modes.⁵³ Peaks between 400 and 600 cm^{-1} are due to the $\delta(\text{O}-\text{W}-\text{O})$ deformation modes, while any Raman peaks occurring below 400 cm^{-1} are WO_3 lattice modes. The most prominent peak of polystyrene exists at 993 cm^{-1} , which corresponds to the polystyrene ν_1 ring-breathing mode.⁵⁴

The WO_3 nanoparticles behaved in a predictable fashion; at lower DEP frequencies the concentration of the particle stream increases while the applied voltage frequency is reduced (as observed in Fig. 3). This trend is reflected in the Raman spectra taken in Fig. 4, which show greater intensity counts for lower DEP frequencies. The Raman intensity observed for the no DEP and 20 MHz conditions were almost identical in magnitude, due to the low concentration of the particle streams in both cases.

Polystyrene particles have distinct Raman peaks in the dehydrated state, when particle concentrations are high.⁵⁴ However once the particles were diluted to 1.5% w/w, and no DEP voltage was applied, the Raman peaks became indistinguishable from the background noise (Fig. 5). Alternatively, when a DEP voltage of 15 V was applied, at frequencies as low as 500 kHz the Raman peaks of polystyrene were present. No significant difference was observed in the polystyrene nanoparticle Raman spectra when frequencies other than 500 kHz were applied. The observation of

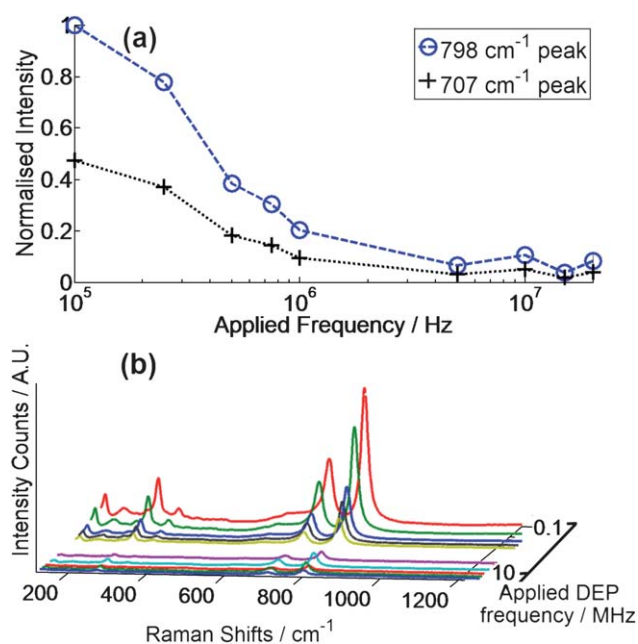


Fig. 4 (a) Plot of normalised WO_3 nanoparticle Raman peak intensity vs. the applied DEP frequency. (b) Plot of WO_3 nanoparticle Raman spectra at different DEP frequencies, decreasing in frequency along the z -axis.

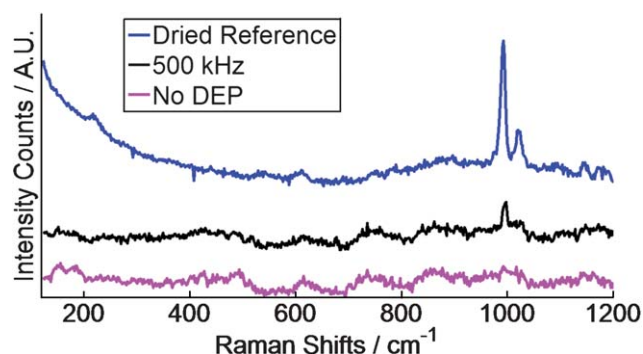


Fig. 5 Plot of polystyrene Raman spectra under various conditions (see legend).

Raman signals, even small in magnitude, is an important outcome. Although the narrow band of polystyrene particles could be hardly visually resolved using the optical microscope, the presence of a Raman signal indicates their presence.

Raman response at varying depths

To investigate the behaviour of particles, and possibly their concentrations, along the depth of the microchannel, the DEP force was held constant by applying an AC signal of 15 V and 500 kHz . This frequency was chosen as it provides the greatest DEP force on the particles. The Raman microscope lens was then focused at different depths within the microchannel.

The possible drawback to this method can be excessive laser light scattering. As the Raman microscope lens is focused deeper into the particle stream, the Raman signals are scattered off more particles. This leads to a reduction in the Raman signal intensity.

Fig. 6(a) shows that the Raman signal from the WO_3 particles decrease as the Raman laser is focused deeper into the microchannel. Fig. 6(b) presents this relationship for both the 798 and 707 cm^{-1} peaks vs. depth. This demonstrates that the DEP force is large enough to overcome the sedimentation force and to push the particles towards the electrodes patterned on the top surface.

Lateral Raman response mapping

Raman spectra were captured from the top surface of the microchannel at varying lateral positions (Fig. 7(a) and (b)). This allows for a deeper understanding of the particle distribution around the electrodes, while experiencing positive DEP forces. In order to quantify the concentration of particles using the Raman pattern peaks, all volume fractions were calculated in % and normalised against the zero DEP field Raman measurement, which corresponds to the 6.5% w/w. We used the intensity of the 6.5% w/w WO_3 peak at 798 cm^{-1} as the reference to estimate the local concentration of particles at other lateral positions. Assuming that the WO_3 concentration increases linearly with the increase of the Raman peak intensity,^{1,9,14,16,55} and that at zero peak intensity we have no particles present, we calculated the local volume fractions of WO_3 at the individual positions. The values can be seen in Table 1.

Fig. 7(c) shows a grey-scale overlay depicting the measured levels of concentration. Interestingly, the figure indicates that the

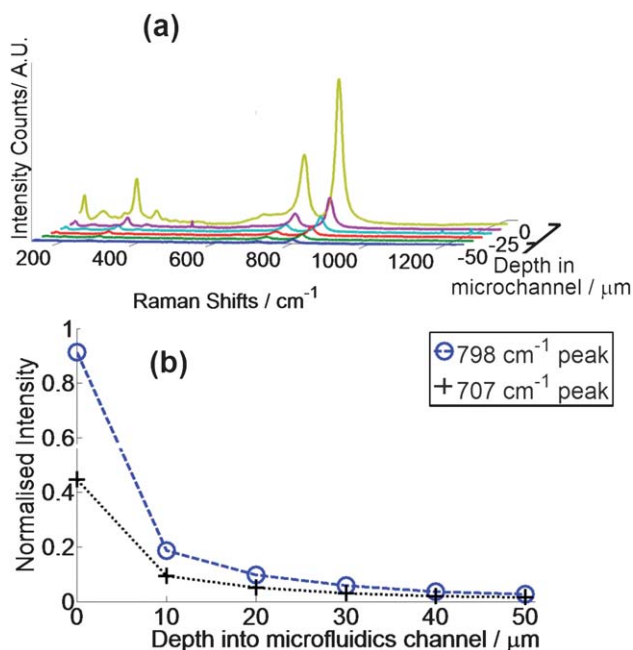


Fig. 6 (a) Plot of WO_3 -polystyrene Raman spectra at varying depths within the microchannel, with a constant DEP force being applied. The closest plot represents the spectra 50 μm deep into the channel; the furthest plot represents the spectra at the top surface of the channel. (b) Plot of WO_3 -polystyrene normalised Raman peak intensity vs. depth within the microfluidics channel.

highest concentration of WO_3 nanoparticles can be found just after the tip of the electrode, at the beginning of the particle stream. These results illustrate the advantage of the Raman measurement, as this could not be discerned from the optical image (Fig. 7(a)). This platform would be even more useful when dealing with completely transparent and non-transparent nanoparticle suspensions, where visual microscopy is impractical. As can be seen, there is no optical contrast on the sides of the narrow band (Fig. 7(a)), although the presence of particles is evidently confirmed by Raman patterns.

The assumption of a linear correlation between Raman intensity and local volume fraction might not hold at high volume fractions, such as that measured at point B (Table 1). There are several reasons for this:

It is possible that at high particle volume fractions, the effective dielectric constant of the medium is altered by the particles. At high volume fractions, the complex permittivity equation can be approximated using:^{56,57}

$$\frac{\varepsilon^* - \varepsilon_m^*}{\varepsilon^* + 2\varepsilon_m^*} \approx \left(\frac{\varepsilon_p^* - \varepsilon_m^*}{\varepsilon_p^* + 2\varepsilon_m^*} \right) \varphi \quad (3)$$

where φ is the volume fraction of the disperse phase, and ε^* is the complex permittivity of the composite. This equation shows the permittivity of the dispersion system, ε^* , changes with volume fraction, and also changes relative to the applied DEP field frequency. Eqn (3) predicts a 25% increase in the intensity of the permittivity at 0.11 WO_3 volume fractions (see ESI†). If the Raman signal also increased by the same factor, the actual WO_3 concentration should be less or equal to 85.2% w/w divided by 1.25 = 68.16% w/w (9.5% v/v).

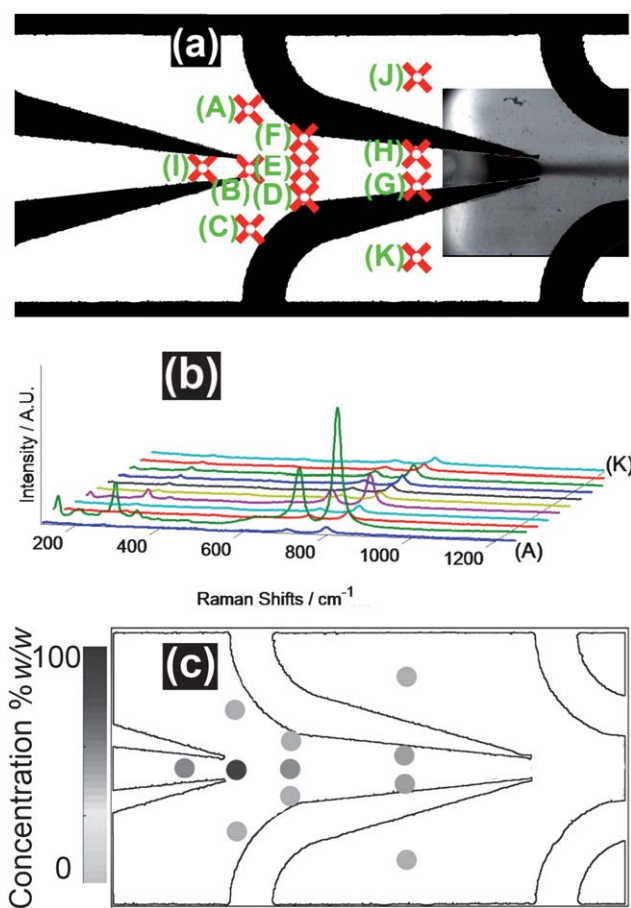


Fig. 7 (a) Locations of Raman measurements. (b) Results of Raman spectroscopy at the varying locations (A–K). (c) Overlay of local concentration values with grey-scale background, values based on Raman spectra intensity.

Alternatively, at low volume fractions only a small percentage of the Raman signal is reflected back to the objective lens. However as the volume fraction increases, the particles are in close proximity to one another, which causes more of the Raman

Table 1 Particle concentrations at the locations in Fig. 7(a)

Position of focal point	Concentration (% w/w) ^a	Concentration (% v/v) ^b
No DEP	6.5	0.91
A	5.7	0.80
B	85.2	11.9
C	6.5	0.91
D	5.9	0.82
E	23.5	3.28
F	5.9	0.82
G	6.0	0.84
H	7.8	1.09
I	10.3	1.44
J	5.9	0.82
K	5.6	0.78

^a Calculated from data in Fig. 7. ^b Calculated using a density of 7.16 g ml^{-1} as per Sigma Aldrich WO_3 datasheet.

signal to reach the objective lens, increasing the signal detected. As a result, the Raman signal intensity for the 6.5% w/w (0.91% v/v) sample received at the detector may not be proportional to the real concentration (see ESI† for further discussion).

Conclusions

In this work, we have demonstrated the capability of a novel microfluidic–Raman system to determine the concentration of suspended nanoparticles. We have verified the ability of the system to perform optical Raman measurements on moving suspended nanoparticles that were manipulated using DEP. With the DEP manipulation, we produced areas of high and low particle concentrations and then implemented a Raman system to assess the type and concentration of the particles.

These simultaneous manipulations and Raman signal observations can be potentially used for understanding some of the fundamental phenomena occurring when particles are suspended in liquid media. Using DEP forces, suspended particles can be brought into close proximity to one another, allowing the exchange of electrons, photons and phonons between them. DEP permits the controlled manipulation of the particle spacing, allowing observations to be made at various particle conditions of interest.

As an analytical tool, such a platform can create many exciting opportunities for research. The platform will allow for *in situ* analysis of particles, without the need to dehydrate the samples before performing Raman spectroscopy.

Future research into this system may include the integration of SERS techniques to amplify the Raman signals of materials that are capable of showing SERS signals such as gold nanoparticles. With the intense research into SERS^{46,58–60} and SERRS,^{61,62} these microfluidic DEP–Raman platforms have the potential for many exciting applications. For example, bio-sensing applications for this platform can be considered when combining SERS and DEP, as DEP can be used for achieving high particle concentration levels required by most optical based measurements for obtaining low detection limits.

References

- B. D. Piorek, S. J. Lee, J. G. Santiago, M. Moskovits, S. Banerjee and C. D. Meinhardt, *Proc. Natl. Acad. Sci. U. S. A.*, 2007, **104**, 18898–18901.
- A. G. Walsh, A. N. Vamivakas, Y. Yin, S. B. Cronin, M. S. Unlu, B. B. Goldberg and A. K. Swan, *Nano Lett.*, 2007, **7**, 1485–1488.
- D. Hou, S. Maheshwari and H. C. Chang, *Biomicrofluidics*, 2007, **1**, 014106.
- M. P. S. de Almeida, K. L. Caiado, P. P. C. Sartoratto, D. Silva, A. R. Pereira and P. C. Morais, *J. Alloys Compd.*, 2010, **500**, 149–152.
- J. Mairhofer, K. Roppert and P. Ertl, *Sensors*, 2009, **9**, 4804–4823.
- A. Ghubade, S. Mandal, R. Chaudhury, R. K. Singh and S. Bhattacharya, *Biomed. Microdevices*, 2009, **11**, 987–995.
- G. Ocvirk, T. Tang and D. J. Harrison, *Analyst*, 1998, **123**, 1429–1434.
- Y. C. Tung, M. Zhang, C. T. Lin, K. Kurabayashi and S. J. Skerlos, *Sens. Actuators, B*, 2004, **98**, 356–367.
- L. X. Chen and J. B. Choo, *Electrophoresis*, 2008, **29**, 1815–1828.
- N. A. Abu-Hatab, J. F. John, J. M. Oran and M. J. Sepaniak, *Appl. Spectrosc.*, 2007, **61**, 1116–1122.
- A. E. Grow, L. L. Wood, J. L. Claycomb and P. A. Thompson, *J. Microbiol. Methods*, 2003, **53**, 221–233.
- F. T. Docherty, P. B. Monaghan, R. Keir, D. Graham, W. E. Smith and J. M. Cooper, *Chem. Commun.*, 2004, (1), 118–119.
- T. Park, S. Lee, G. H. Seong, J. Choo, E. K. Lee, Y. S. Kim, W. H. Ji, S. Y. Hwang and D. G. Gweon, *Lab Chip*, 2005, **5**, 437–442.
- R. Wilson, S. A. Bowden, J. Parnell and J. M. Cooper, *Anal. Chem.*, 2010, **82**, 2119–2123.
- Y. S. Huh, A. J. Lowe, A. D. Strickland, C. A. Batt and D. Erickson, *J. Am. Chem. Soc.*, 2009, **131**, 2208–2213.
- L. X. Quang, C. Lim, G. H. Seong, J. Choo, K. J. Do and S. K. Yoo, *Lab Chip*, 2008, **8**, 2214–2219.
- R. Keir, E. Igata, M. Arundell, W. E. Smith, D. Graham, C. McHugh and J. M. Cooper, *Anal. Chem.*, 2002, **74**, 1503–1508.
- K. R. Ackermann, T. Henkel and J. Popp, *ChemPhysChem*, 2007, **8**, 2665–2670.
- S. Lee, S. Joo, S. Park, S. Kim, H. C. Kim and T. D. Chung, *Electrophoresis*, 2010, **31**, 1623–1629.
- L. M. Tong, M. Righini, M. U. Gonzalez, R. Quidant and M. Kall, *Lab Chip*, 2009, **9**, 193–195.
- C. Zhang, K. Khoshmanesh, F. J. Tovar-Lopez, A. Mitchell, W. Wlodarski and K. Kalantar-zadeh, *Microfluid. Nanofluid.*, 2009, **7**, 633–645.
- C. J. L. Constantino, T. Lemma, P. A. Antunes and R. Aroca, *Anal. Chem.*, 2001, **73**, 3674–3678.
- K. H. Bhatt and O. D. Velev, *Langmuir*, 2004, **20**, 467–476.
- S. Fiedler, S. G. Shirley, T. Schnelle and G. Fuhr, *Anal. Chem.*, 1998, **70**, 1909–1915.
- K. Khoshmanesh, C. Zhang, F. J. Tovar-Lopez, S. Nahavandi, S. Baratchi, A. Mitchell and K. Kalantar-Zadeh, *Microfluid. Nanofluid.*, 2010, **9**, 411–426.
- B. H. Lapizco-Encinas, B. A. Simmons, E. B. Cummings and Y. Fintschenko, *Anal. Chem.*, 2004, **76**, 1571–1579.
- B. H. Lapizco-Encinas, B. A. Simmons, E. B. Cummings and Y. Fintschenko, *Electrophoresis*, 2004, **25**, 1695–1704.
- H. A. Pohl and J. S. Crane, *Biophys. J.*, 1971, **11**, 711–727.
- N. G. Green and H. Morgan, *J. Phys. D: Appl. Phys.*, 1997, **30**, L41–L44.
- K. Kalantar-zadeh, K. Khoshmanesh, A. A. Kayani, S. Nahavandi and A. Mitchell, *Appl. Phys. Lett.*, 2010, **96**, 101108.
- A. A. Kayani, C. Zhang, K. Khoshmanesh, J. L. Campbell, A. Mitchell and K. Kalantar-zadeh, *Electrophoresis*, 2010, **31**, 1071–1079.
- S. Y. Lee, T. H. Kim, D. I. Suh, N. K. Cho, H. K. Seong, S. W. Jung, H. J. Choi and S. K. Lee, *Chem. Phys. Lett.*, 2006, **427**, 107–112.
- D. Q. Wang, R. Zhu, Z. Y. Zhou and X. Y. Ye, *Appl. Phys. Lett.*, 2007, **90**, 103110.
- H. A. Pohl, *Dielectrophoresis*, Cambridge University Press, Oklahoma, 1978.
- C. Zhang, K. Khoshmanesh, A. Mitchell and K. Kalantar-zadeh, *Anal. Bioanal. Chem.*, 2010, **396**, 401–420.
- K. Khoshmanesh, C. Zhang, F. J. Tovar-Lopez, S. Nahavandi, S. Baratchi, K. Kalantar-Zadeh and A. Mitchell, *Electrophoresis*, 2009, **30**, 3707–3717.
- S. C. Bae, H. Lee, Z. Lin and S. Granick, *Langmuir*, 2005, **21**, 5685–5688.
- T. Matsue, N. Matsumoto and I. Uchida, *Electrochim. Acta*, 1997, **42**, 3251–3256.
- M. Suzuki, T. Yasukawa, Y. Mase, D. Oyamatsu, H. Shiku and T. Matsue, *Langmuir*, 2004, **20**, 11005–11011.
- E. C. Ziemath and M. A. Aegerter, *J. Mater. Res.*, 1994, **9**, 216–225.
- A. Kumatani and P. A. Warburton, *Appl. Phys. Lett.*, 2008, **92**, 243123.
- N. Takano, L. M. Doeswijk, M. A. F. van den Boogaart, J. Auerswald, H. F. Knapp, O. Dubochet, T. Hessler and J. Brugger, *J. Micromech. Microeng.*, 2006, **16**, 1606–1613.
- D. Krishnamurti, *Proc. Math. Sci.*, 1958, **47**, 276–291.
- R. Krupke, S. Linden, M. Rapp and F. Hennrich, *Adv. Mater.*, 2006, **18**, 1468–1470.
- C. G. Xie and Y. Q. Li, *Appl. Phys. Lett.*, 2002, **81**, 951–953.
- K. R. Strehle, D. Cialla, P. Rosch, T. Henkel, M. Kohler and J. Popp, *Anal. Chem.*, 2007, **79**, 1542–1547.
- G. Roman and C. Culbertson, *Langmuir*, 2006, **22**, 4445–4451.
- J. C. Daigle and J. P. Claverie, *J. Nanomater.*, 2008, **2008**, 609184, pages 1–8.
- S. Verma, R. Gokhale and D. J. Burgess, *Int. J. Pharm.*, 2009, **380**, 216–222.
- A. G. Souza, J. Mendes, V. N. Freire, A. P. Ayala, J. M. Sasaki, P. T. C. Freire, F. E. A. Melo, J. F. Juliao and U. U. Gomes, *J. Raman Spectrosc.*, 2001, **32**, 695–699.

- 51 X. Y. Ma, J. Q. Lu, R. S. Brock, K. M. Jacobs, P. Yang and X. H. Hu, *Phys. Med. Biol.*, 2003, **48**, 4165–4172.
- 52 E. Washizu, A. Yamamoto, Y. Abe, M. Kawamura and K. Sasaki, *Solid State Ionics*, 2003, **165**, 175–180.
- 53 M. F. Daniel, B. Desbat, J. C. Lassegues, B. Gerand and M. Figlarz, *J. Solid State Chem.*, 1987, **67**, 235–247.
- 54 C. Barthet, S. P. Armes, S. F. Lascelles, S. Y. Luk and H. M. E. Stanley, *Langmuir*, 1998, **14**, 2032–2041.
- 55 H. Chon, C. Lim, S. M. Ha, Y. Ahn, E. K. Lee, S. I. Chang, G. H. Seong and J. Choo, *Anal. Chem.*, 2010, **82**, 5290–5295.
- 56 K. Asami, T. Hanai and N. Koizumi, *Jpn. J. Appl. Phys.*, 1980, **19**, 359–365.
- 57 C. Boned, J. Peyrelasse, M. Clausse, B. Lagourette, J. Alliez and L. Babin, *Colloid Polym. Sci.*, 1979, **257**, 1073–1082.
- 58 T. Chen, H. Wang, G. Chen, Y. Wang, Y. H. Feng, W. S. Teo, T. Wu and H. Y. Chen, *ACS Nano*, 2010, **4**, 3087–3094.
- 59 T. M. Cotton, J. H. Kim and G. D. Chumanov, *J. Raman Spectrosc.*, 1991, **22**, 729–742.
- 60 M. Graff, J. Bukowska and K. Zawada, *J. Electroanal. Chem.*, 2004, **567**, 297–303.
- 61 K. Kneipp, Y. Wang, R. R. Dasari and M. S. Feld, *Appl. Spectrosc.*, 1995, **49**, 780–784.
- 62 C. H. Munro, W. E. Smith, M. Garner, J. Clarkson and P. C. White, *Langmuir*, 1995, **11**, 3712–3720.